

# Analysis and Flow Regime Identification of Bubble Column Dynamics

M.A. Bennett, S. P. Luke, X. Jia, R.M. West and R.A. Williams

Camborne School of Mines, University of Exeter, Redruth, Cornwall, TR15 3SE, UK,  
email : mabennet@csm.ex.ac.uk

The authors are members of The Virtual Centre for Industrial Process Tomography

**Abstract** - Bubble columns are widely used across a range of industries. The work described in this paper, although applied to minerals separation flotation columns, is equally applicable in the wider context of bubble columns. In flotation columns a number of flow regimes may be obtained and are difficult to visualise and detect. An Electrical Capacitance Tomography (ECT) sensor has been applied to investigate the potential of ECT for flotation column visualisation and control. Different methods of flow regime analysis are reported including a repeatable and robust analytical procedure that has been designed to quantify heterogeneity.

**Keywords:** bubble columns, ECT, multi-phase flow.

## 1. INTRODUCTION

Several attempts have been reported to use electrical capacitance tomography (ECT) to visualise two phase and three phase flows, as reviewed by Reinecke *et al.* [1]. To a lesser extent tomographic data has been used to characterise flows, for example in trickle bed reactors [2] and pneumatic conveying [3] [4].

In this paper, the use of ECT is examined for distinguishing homogeneous bubble flow and churn flow. Then a quantification of these flow regimes is compared to simple secondary parameters (derived from multiple frame measurements) obtained from images and capacitances. A wide variety of conditions were created to test the viability of the method using different spargers, frother concentrations, and height between sparger and sensor.

It was realised that aside from the actual flow regime there were many inter-related aspects of flow that contributed to the sensor measurement including bubble size and size distribution, bubble swarming and radial gas concentration (radial profile). Due to its high sensitivity and low noise, it was also believed that the sensor showed promise in highlighting further more detailed aspects of flow and these were investigated.

Further work involved constructing radial profiles from statistics applied to the different orientation of capacitances, assessing the sensors ability to distinguish bubble size, and also a new tool for assessing and interpreting flow is introduced: the Heterogeneity Index for pixel-based Tomograms.

## 2. EXPERIMENTAL APPARATUS

A flow regime transition will occur when a change in flowrate results in a change in the type of flow regime. A typical way of assessing flow regime transitions, is to graph the gas-flowrate (flowrate) against the gas holdup ( $\epsilon_m$ ) and judge the flow regime from the overall relationship between these [5].

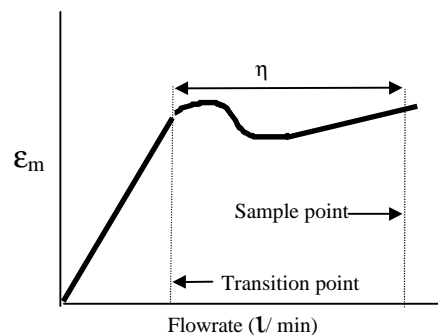
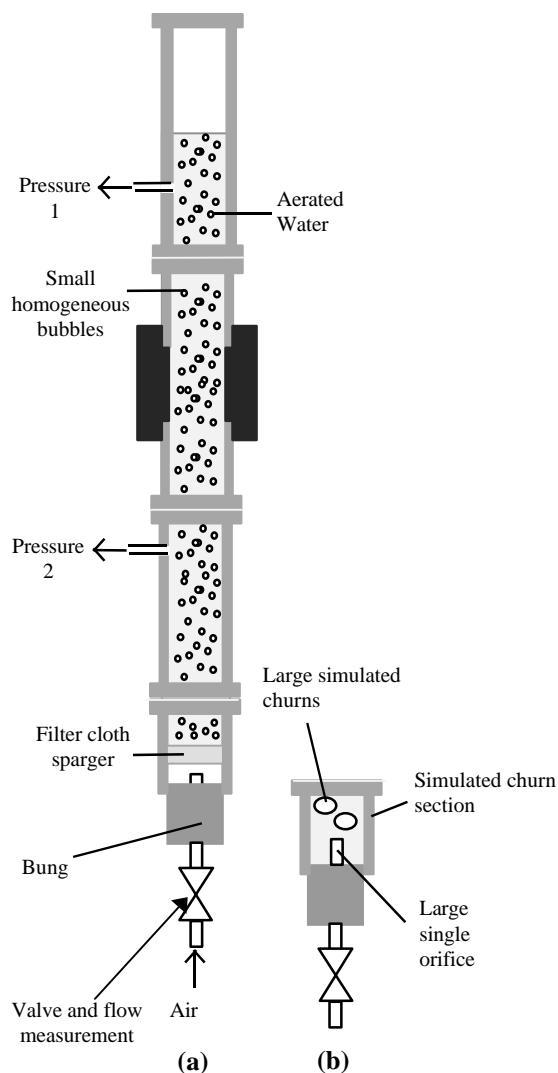


Figure 1: An idealised gas-flowrate against gas fraction graph

In this paper a series of sensor measurements taken at different gas-flowrates under the same column conditions of solution type, sparger and distance from the sparger and sensing zone is called a set. In taking the measurements for a set, the flowrate is incrementally increased between successive measurements. From calibration a mean value of the gas voidage in the sensing region can be deduced and used to construct a flow curve such as in Figure 1 [4]. Sensor measurements consists of data taken for 30 seconds and at one hundred frames per second (3000 frames- each based on dielectric pair measurements).



**Figure 2: The apparatus used for flow regime production**

The water used is double distilled, the width of the column inner diameter 56 mm, and the length 102.5 cm. Initial experimentation involved comparing two very different sets. Figure 2 shows the experimental apparatus needed to reproduce various types of flow ranging from gentle bubbling to a simulated churn flow.

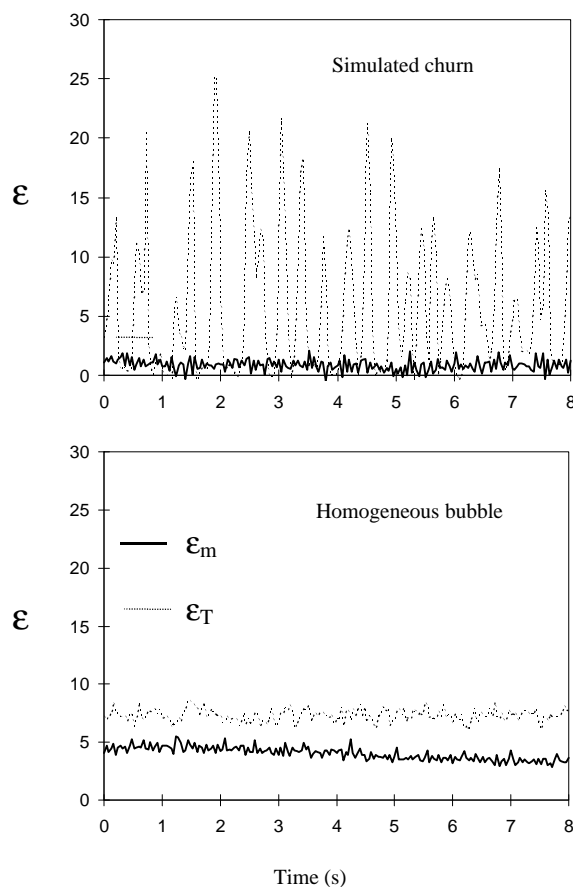
Figure 2 (a) shows the apparatus in 'column' mode with a suitable portable section containing a selected sparger of filter cloth on a metal grill. There are also two pressure points to give an additional means of gas concentration measurement. An increase in gas-flowrate was capable of giving an ideal succession of flow regimes, from homogeneous bubble flow, transition and then churn flow. During homogeneous bubble flow the individual bubbles produced were judged to be smaller in dimension than the resolution of the sensor and individual bubbles were very unlikely to be imaged directly.

Figure 2 (b) shows the alternative section needed to produce churn flow containing a single

orifice for the passage of gas into the section. The purpose of this set was to achieve a churn set uncontaminated by homogeneous bubble flow. Even at the lowest flows the churns produced were similar in dimension to the limit of the resolution of the sensor and very likely to be imaged directly. The churns were produced by forcing gas through a single glass tube (3 mm diameter).

### 3. INITIAL COMPARISONS

Homogeneous bubble flow and simulated churn flow regimes were compared, both of them being extremes.



**Figure 3: Gas voidage estimate derived from pressure hold-up ( $\epsilon_m$ ) and capacitance imaging ( $\epsilon_T$ ) for a flowrate of 1 l/min**

In assessing the results firstly comparisons are made between pressure measurement giving the actual gas hold-up ( $\epsilon_m$ ) and the corresponding sensor measurement ( $\epsilon_T$ ) over time. These are compared in Figure 3 for both churn and homogeneous bubble flow over an 8 second time period, before examining three-dimensional reconstructions of the sensor images obtained.

It can be assumed from these observations that the sensor has strong potential for assessing flow regime. This potential is examined in more detail by using three-dimensional reconstructions.

These are in the form of isocontours. One hundred frames, representing 4 seconds of data are used.

In Figure 4 the isocontours obtained for both the simulated churn flow and homogeneous bubble flow are shown at differing flowrates. It can be seen in the simulated churn flow reconstructions that discrete distributions occur bearing a very strong likeness to churns, these also become more frequent and larger for higher flowrates. On the other hand for homogeneous bubble flow, discrete distributions are not apparent.

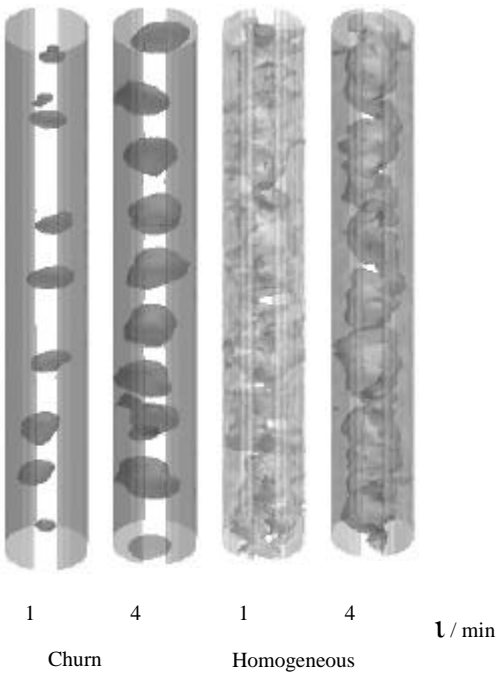


Figure 4: Isocontours of homogeneous bubble and churn flow for the gas-flowrates

A good measure of the sharpness of isocontour thresholds can also be gained by using axial slices of the data [4].

#### 4. UNIVERSAL QUANTIFICATION OF FLOW REGIME

Combinations of spargers, frother concentrations, flowrate and height were used to give a range of conditions for analysis work using the same experimental apparatus as shown in section 2.

In practise the definitions of flow regime are often quite unclear, with latest research pointing to up to five regimes, and additional gradual transitions between them [6]. Often the transition between these processes is difficult to define rigidly over the small incremental changes in flowrate between measurements in these sets, but when considering the full range of the flowrate values in a set, the errors in identifying flow

regime are negligible. It was decided to use the flow curve for defining flow regime in individual measurements to distinguish homogeneous bubble flow and churn flow.

The point where transition occurs in the flow curve was decided as the flowrate where the  $\epsilon_T$  value for the measurement deviates from the initial straight line from the origin. Assessing the flow transition point by this method is a reasonably quantitative process using  $\epsilon_T$  as can be seen in Figure 5.

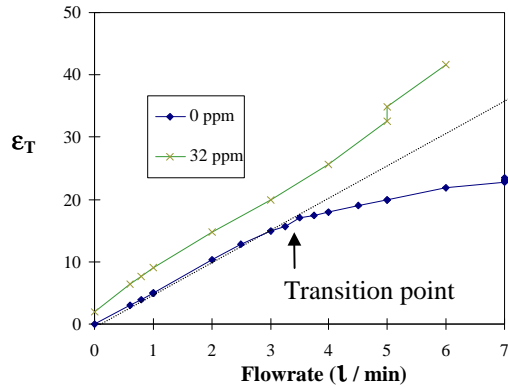


Figure 5: The  $\epsilon_T$  values obtained for different flowrates and frother concentrations for a sparger of plain filter cloth, showing definitions of transition point

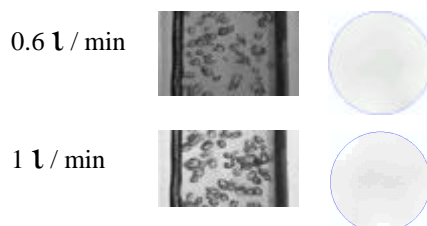
The flow curves are shown for the filter cloth sparger at frother concentrations of 0 and 32 ppm in Figure 5. It is obvious that a transition occurs at 0 ppm, but not at 32 ppm.

Figure 6 shows typical video snapshots adjacent to corresponding sensor images at different flowrates for at 0 ppm and 32 ppm. At 0 ppm the transition from homogeneous bubble flow to churn flow can be easily seen occurring gradually. In the 32 ppm set, as the flowrate and bubble density in the video snapshots increases, there is a lowering of  $\epsilon_T$  in the sensor images but no sign of churns in either sensor or video data, as expected.

The obvious change in homogeneity can be quantified using the mean from all the images in a measurement, of the standard deviation of the pixel values (Image sd), which is shown for the two flow curves in Figure 7.

It can be seen that the flow curve for 0 ppm shows a significant increase for transition, while 32 ppm does not, agreeing with the trends seen in Figure 6.

Considering the often gradual change of flow regime with flowrate increase, a quantitative



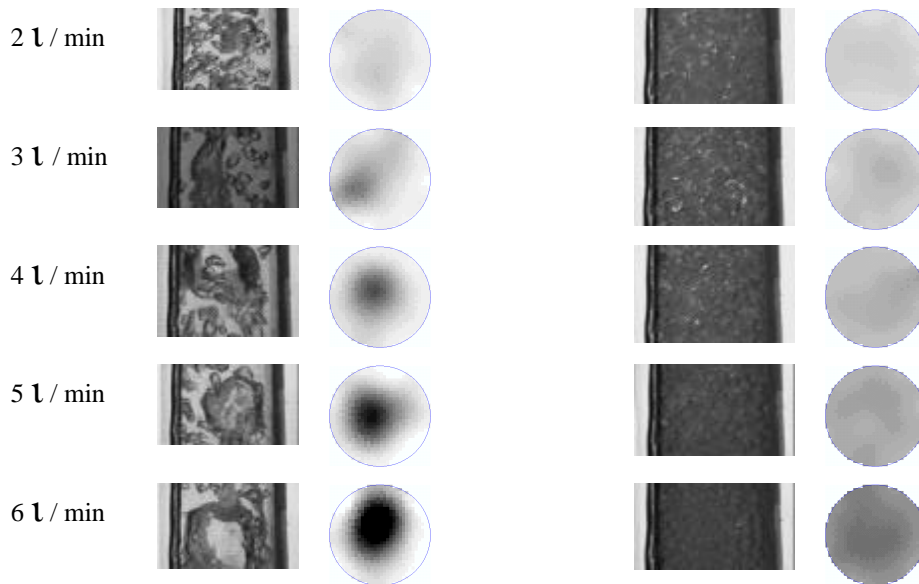


Figure 6: Video (left) and sensor images (right) of flow regimes over different flowrates for (a) 0 ppm - transition (b) 32 ppm - no transition

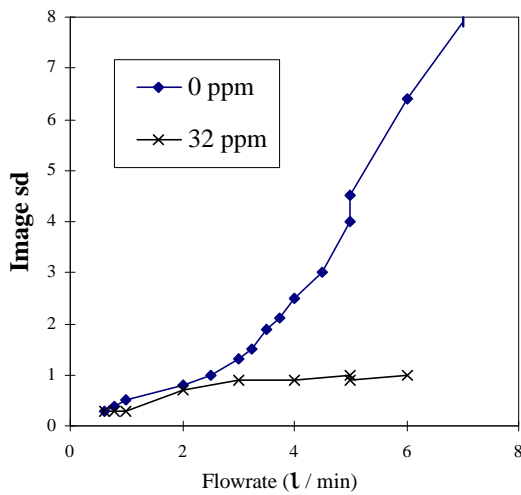


Figure 7: The Image sd for different frother concentrations and gas-flowrates

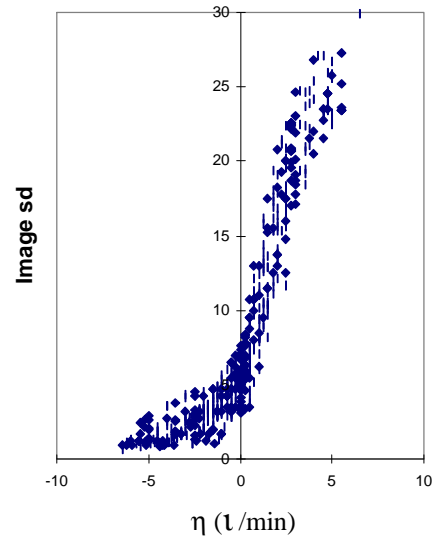
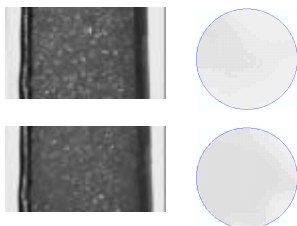


Figure 8: Image sd used as a quantification of flow regime.

estimation of flow regime is then constructed by using flow definitions from the flow curve, for example,  $\eta$  as the current magnitude of flow rate either side of the transition point (see Figure 1).

Quantification of flow regime using Image sd compared to  $\eta$  for a variety of sets is shown in Figure 8.

The Image, sd, appears reasonably universal in distinguishing flow regime quantitatively, despite human error inevitable in the designation of flow regime and the wide range of data used, and from this it can be assumed that the sensor shows potential in quantifying flow regime, but it is evident that quantification is far more likely with churn flow, than with homogeneous bubble flow.



## 5 RADIAL GAS CONCENTRATION PROFILES

Another way in which the sensors ability to supply information on flow can be utilised is in radial profile imaging of the gas fraction. This can be shown in a useful and quick way by calculating the mean of capacitances of the same class. Class is defined as the spacing between the two electrodes used to measure the capacitance, as demonstrated by Figure 9.

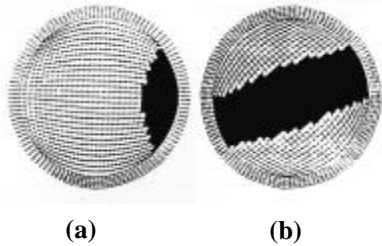


Figure 9: Interelectrode capacitances (a) class 1 - adjacent electrodes (b) class 6 - opposite electrodes

Radial profiles are now shown for a filter cloth sparger at frother concentrations of 0 ppm and 32 ppm in Figures 10, giving a demonstration of radial profile change (expressed as  $\epsilon_c$  for each class ( $\epsilon_c$ )) with an increase in flowrate.

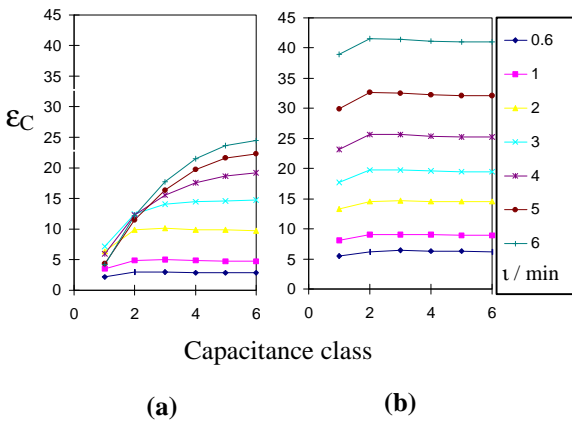


Figure 10: Radial profile change with flowrate increase for the filter cloth sparger at (a) 0 ppm (b) 32 - ppm

In Figure 10 (a) it can be seen that the constructed radial profile from initially being flat at low flowrates becomes more bow shaped and steep at the edges as the flow regime assignment changes from homogeneous bubble flow to churn flow. It can also be seen by observing the change with flowrate that flow regime transition is a gradual one. For homogeneous bubble flow, looking at Figure 10 (b) for 32 ppm, it can be seen that for all the flowrates, the constructed radial profile remains relatively flat.

The characteristic shapes for two different spargers, one of filter cloth, and one of rubber are

now studied using a flowrate of 1 l / min, and frother concentrations of 0, 4, 16 and 32 ppm, in

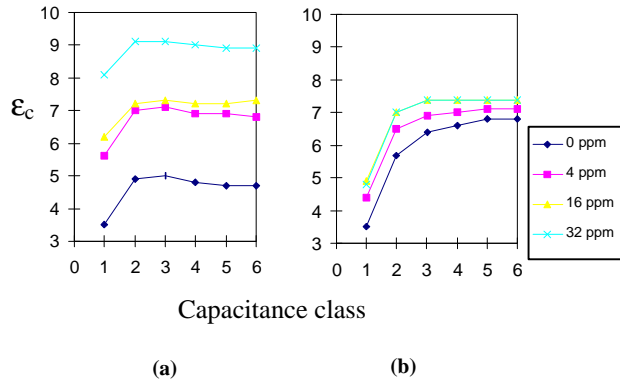


Figure 11: Radial profile constructions for different frother concentrations using (a) the plain cloth sparger (b) the rubber sparger

Figures 11 (a) and 11 (b) respectively.

It is clear, that despite the change in frother concentration and class gas fractions, that the shapes retain essentially the same structure for a sparger at different frother concentrations. Figure 11 (a) shows a steep dip in the constructed radial profile edge, but after this there is a small rise towards the centre. The rubber sparger in Figure 11 (b) appears to show a more bow shaped type of radial profile.

It can be seen from Figure 10 that the sensor has shown a good ability in showing constructed radial profile differences for different flow types, and from Figure 11 it appears to identify aspects of radial profile specific for individual spargers. Also trends in Figure 10 show agreement with the flow regimes. This could be a potentially valuable tool in supplying flow regime information, and for sparger testing and the detection of faults.

## 6. BUBBLE SIZE

It was realised that there was a possibility of the sensor recognising aspects of the bubble size of a homogeneous bubble flow regime. Given the number of bubbles and their size in such a regime it was unlikely that they would be imaged individually and directly. A number of bubbles of a certain size were capable of leaving a 'fingerprint' or 'texture' on the image which could then be analysed by simple variables.

Data was taken at 1 l / min from a variety of spargers and frother concentrations and in processing the data obtained from each flow set, five instantaneous video snapshots were taken at random from each measurement, and from each of these video snapshots, the three largest most significant bubbles were highlighted and the two largest perpendicular dimensions of each were measured. The mean was then taken of the thirty measurements to give a significant bubble value -  $x_{SB}$ . Essentially  $x_{SB}$  is an estimation of the size of

significant bubbles at the larger end of the bubble size distribution.

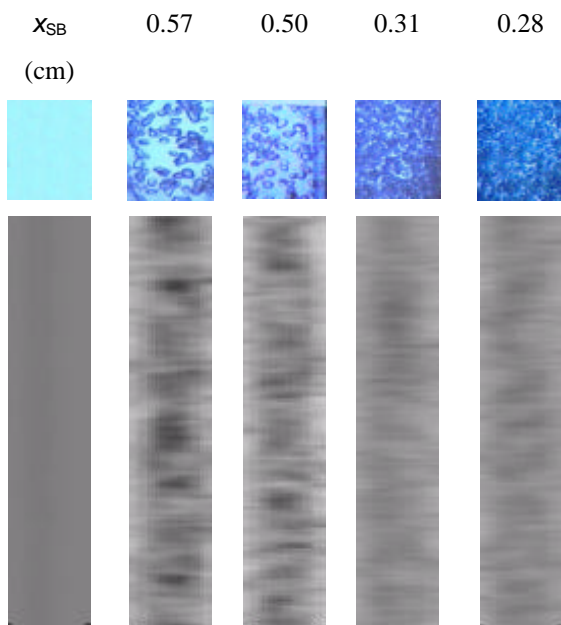


Figure 12: Video frames and axial slices illustrating bubble size

Figure 12 shows typical video snapshots and corresponding four second central slices for large and small  $x_{SB}$  values using different spargers, the two on the left are larger bubble sizes, while those on the right are smaller. Axial slices are scaled from  $\epsilon_T$  values of 25 to -5.

In the axial slices, it can be seen that the two on the left, representing larger bubbles, give a significantly textured image, while those on the right, representing smaller bubbles do not. Although the bubbles are not being imaged directly this demonstrates the potential use of the sensor in distinguishing bubble size. It can also be seen that a reconstruction of zero flowrate shows nothing significant, and it can be assumed that even at high homogeneities, patterns in the flow are still being imaged.

Utilising this information graphs can be shown of secondary parameters from images and capacitances against the  $x_{SB}$  value. The Image sd, and the mean of all the frames in a measurement of capacitance class 6 (Class 6 sd) are now shown in Figures 13 and 14 respectively.

All the graphs show that the  $x_{SB}$  value is distinguishable for bubble sizes of 0.6 cm to 0.4 cm, and a reasonably clear trend is seen in each of them. Interestingly the capacitance based secondary parameter show the slightly better distinguishing ability, despite its simplicity. One possible reason for this is that this measured value as a standard deviation of radially symmetrical sensitivity maps is not directly affected by radial gas concentration, unlike the Image sd.

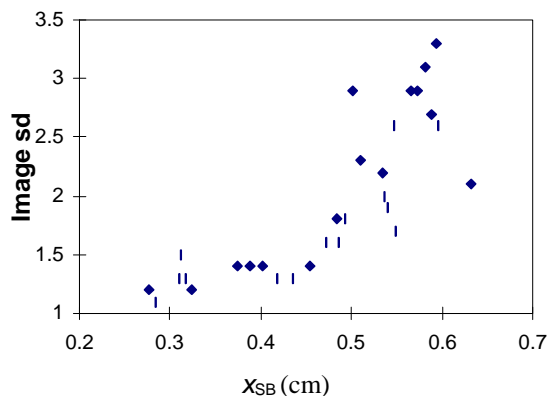


Figure 13: The Image sd compared with  $x_{SB}$

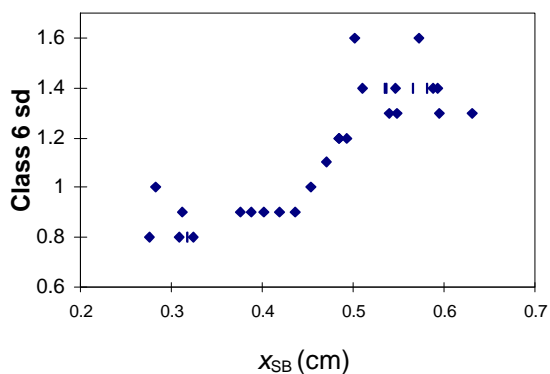


Figure 14: The Class 6 sd compared with  $x_{SB}$

## 7. THE HIT STATISTIC

This section covers an investigation of an index of heterogeneity, HIT (Heterogeneity Index for pixel-based Tomograms), that was specifically designed for tomogram analysis. Heterogeneity is investigated with reference to a mesh (or grouping of pixels). In this case the single mesh (carefully chosen to match the sensor geometry) shown in Figure 15. Pixel values (permittivity values for ECT) are first ranked, so creating an index independent of scaling. The value reported for the HIT statistic will have a small value when the flow through the sensor is homogeneous and increase for turbulent flows producing a heterogeneous cross section.

It is now shown being applied to the two spargers previously examined in radial profile construction, over a range of flowrates and frother concentrations ( 4 and 16 ppm) in Figures 16 and 17.

For both spargers, 4 ppm is a transition while 16 ppm remains homogeneous.

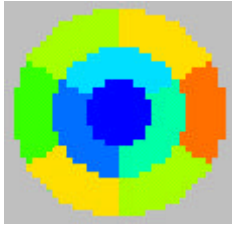


Figure 15: The mesh implemented with the HIT statistic

The values registered by the HIT statistic could potentially be due to many factors because of the amount of information that goes into its product value, the HIT statistic is capable of giving very individual values for individual flows, and some of these are explainable, and some not without further investigation.

There were a number of aspects of measurement that were seen as having a possibility of affecting the HIT value apart from the actual flow regime type. Unwanted factors such as noise and softfield error that were considered negligible and wanted factors such as subtle flow properties within the regime (mentioned earlier), factors such as radial profile, bubble size and distribution, as well as bubble swarming and sparger pulsing could all potentially affect the HIT statistic value.

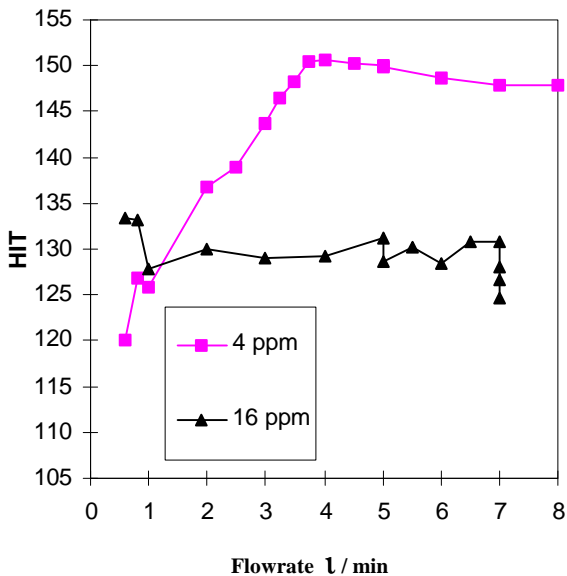


Figure 16: The HIT statistic for the filter cloth sparger

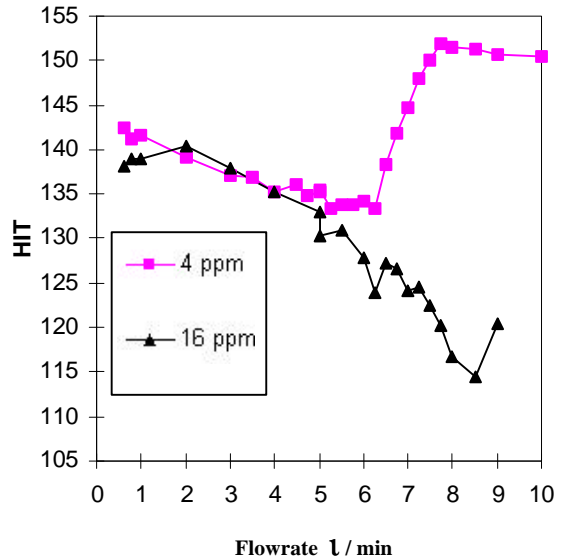


Figure 17: The HIT statistic for the rubber sparger

The HIT statistic shows definite repeatable trends for all the flow sets shown

The first and most important thing to note is that the HIT statistic has higher values for churn than for homogeneous bubble flow. From the nature of the HIT statistic this is expected and shows its general ability in detecting flow regime type. Additionally the HIT values for the highest flowrates where transition to churn occurs (the maximum amount of churn flow measured) are all between 145 and 153, this shows a strong universality for the HIT statistic in registering strong churn flow regime.

In the transition sets, a small inflection occurs in a mainly gradual change at 4ppm for the filter cloth sparger and a large inflection is seen at 4 ppm for rubber. Additionally for non transition sets that are known to remain homogeneous (both spargers at 16 ppm) the inflection becomes a continuous downward slope.

A possible reason for these effects is that as the gas flow is increased and the homogeneous bubble flow does not change its properties significantly - apart from an increase in bubbles, then the greater number of bubbles, statistically, will produce a lower heterogeneity. This is where the autoscaling aspects of the HIT statistic can be quite useful, using variables that are affected by the permittivity scales involved in the flow e.g. Image sd), tends to produce a slight increase for these phases, which does not occur for the HIT statistic.

In general the HIT statistic performs well compared with expectations of being able to distinguish between homogeneous bubble flow and churn flow. It is important to note again however, that there are definite individualistic trends within the values of each flow set and a number of factors about the flow can affect the heterogeneity measurement given by the HIT

statistic, but this is the price that has to be paid for its complex utilisation of the image.

This can have both advantages and disadvantages depending on application. If applied to situations where calibration is impractical and full interpretation of the HIT statistic is possible, this could be an extremely useful tool, especially in measuring subtleties of flow regime. It could also be interacted with scaled measurements and other HIT meshes to supply an array of information with relatively easy interpretation (such as a two or three ring mesh for radial profile information).

## 8. CONCLUSIONS

In this paper the sensors ability to distinguish aspects of flow in detail has been investigated, it has been shown that a reasonable quantification of flow regime using image secondary parameters is possible and that constructed radial profiles from the different classes of capacitance measurements can give information on flow. An individualistic method for flow recognition without a need for calibration has been shown to be a useful tool for future use in assessing and interpreting flow regimes. The sensor was also taken to the limits of its ability where it was used to show potential in distinguishing bubble size in homogeneous bubble flow. It may be concluded that -

ECT can be used to obtain information on -

- Flow regime
- Bubble size
- Gas concentration radial profile
- Flow heterogeneity

in liquid/gas flows in bubble columns and flotation processes where conductivity is low.

Due to its high speed this has applications in the areas of both -

- Monitoring and control
- Testing

## REFERENCES

- [1] N. Reinecke, G. Petritsch, D. Schmitz and D. Mewes, *Tomographic imeasurement techniques - visualization of multiphase flows*, Chemical Engineering and Technology, 21 (1998) 7-18
- [2] N. Reinecke and D. Mewes, *Tomographic imaging of trickle bed reactors*, Chemical Engineering Science, 51 (1996) 2131-2138
- [3] K Ostrowski, S P Luke, M A Bennet and R A Williams, *Real time visualisation and analysis of dense phase powder conveying*, Powder Technology, in press.
- [4] M.A. Bennett, Ph.D.thesis, University of Exeter, to be submitted.
- [5] J.A. Finch, and G.S. Dobby, (1990) *Column Flotation*, Pergamon Press PLC, Oxford
- [6] P.L. Spedding, G.S. Woods, R.S. Raghunathan and J.K. Watterson, *Vertical two-phase flow - Part I: Flow regimes*, Chemical Engineering Research and Design, 76 (1998) 612-619